Electronic Supplementary Information (ESI):

Synthesis of zeolite Y from natural aluminosilicate minerals for fluid catalytic cracking application

Tiesen Li,[‡a] Haiyan Liu,[‡b] Yu Fan,*[a] Pei Yuan,[a] Gang Shi,[a] Xiaotao T. Bi,[c] Xiaojun Bao*[b]

[a]*State Key Laboratory of Heavy Oil Processing, China University of Petroleum, No. 18 Fuxue Road, Changping, Beijing 102249, China.*
[b]*The Key Laboratory of Catalysis, China National Petroleum Corporation, China University of Petroleum, No. 18 Fuxue Road, Changping, Beijing 102249, China.*
[c]*Department of Chemical & Biological Engineering, University of British Columbia, 2360 East Mall, Vancouver, B.C. V6T 1Z3, Canada.*

Supplementary Methods

1. Materials

The natural kaolinite used in this study was a commercial grade product purchased from China Kaolin Clay Company. The natural diatomite mineral used in the present study was purchased from Qingdao Chuanyi Diatomite Company (China). Both of the kaolinite and diatomite minerals were used as received without further purification. Silica sol (containing 25.0 wt% SiO_2) was purchased from Qingdao Haiyang Chemical Company, Ltd. (China). Aluminum sulfate (containing 99.0 wt% $Al_2(SO_4)_3 \cdot 18H_2O$), sodium hydroxide (containing 96.0 wt% NaOH) and sodium aluminate (containing 45.0 wt% Al_2O_3) were purchased from the market. Commercial zeolites Y and ZSM-5 were purchased from Nankai University Catalyst Company (Tianjin, China).

2. Activation of minerals, synthesis of structure-directing agent (SDA) and zeolite, and preparation of catalysts

Activation of the kaolinite and diatomite minerals. In a typical experiment, 37.8 g of the raw kaolinite and 61 g of NaOH powder were mixed in an open-top stainless steel crucible, then 200 mL of water was added giving a high-concentration alkali solution (HCAS) of 15 M NaOH, and finally the resulting mixture of kaolinite-NaOH-H_2O was treated at 200 ^oC with air recirculation for 2 hours to yield the HCAS activated kaolinite. The diatomite

mineral was activated by heating the raw diatomite to 600 ^{o}C at a rate of 2 ^{o}C/min and maintaining at 600 ^{o}C for 2 hours in a muffle furnace with air recirculation. The thermally activated kaolinite sample was obtained by heating the raw kaolinite mineral to 800 ^{o}C at a rate of 2 ^{o}C/min and then maintaining at 800 ^{o}C for 4 hours in an oven with air recirculation.

SDA preparation. Initially, a SDA with a molar composition of 17 SiO_2: Al_2O_3: 17 Na_2O: 350 H_2O was prepared by adding NaOH, $Al_2(SO_4)_3$ ·18 H_2O and deionized water into a silica sol (25 wt%). This solution was aged for 2 days at room temperature.

Synthesis of zeolite Y. 5.6 g of the HCAS activated kaolinite sample was mixed with 7.0 g of the thermally activated diatomite, followed by the addition of 45.0 g of deionized water and 7.0 g SDA under stirring. Then, the resulted mixture was aged for 16 hours at 60 ^{o}C under stirring and then maintained at 100 ^{o}C for 24 hours. Finally, the crystallization product was recovered by washing with deionized water and drying at 120 ^{o}C.

Synthesis of zeolite Y from the thermally activated kaolinite and thermally activated diatomite. 2.26 g of the thermally activated kaolinite sample was mixed with 7.0 g of the thermally activated diatomite, followed by the addition of 45.0 g of deionized water, 7.0 g of SDA and 3.64 g of the NaOH powder under stirring. Then, the resulted mixture was aged for 16 hours at 60 ^{o}C under stirring and maintained at 100 ^{o}C for 24 hours. Finally, the crystallization product was recovered by washing with deionized water and drying at 120 ^{o}C.

Catalyst preparation. The as-synthesized zeolite and a commercial Y-type zeolite were converted to the HY form by successive ion exchanges with a 1.0 M NH_4Cl solution and calcinations at 550 ^{o}C for 2 hours. Then, a mixture consisting of 25 wt% HY, 10 wt% HZSM-5, 50 wt% kaolin clay, water glass and an appropriate amount of water was prepared, extruded to bars of 1.5 mm in diameter, and calcined at 500 ^{o}C for 4 hours. Finally, the bars were crushed and sieved to obtain catalyst particles of 70~150 μm in size. To simulate the commercial deactivation process, the FCC catalysts prepared were deactivated with 100% water vapor at 800 ^{o}C for 10 hours.

3. Characterizations

X-ray photoelectron spectroscopy (XPS). XPS characterization was performed on a Thermo Scientific K-Alpha instrument with a beam size of 400 μm.

Raman spectroscopy. Raman spectroscopy characterization was performed with a Laser Confocal Micro-Raman Spectroscope using 532-nm laser excitation at ambient temperature.

Magic angle spinning nuclear magnetic resonance (MAS NMR) spectroscopy. The

^{27}Al and ^{29}Si MAS NMR spectroscopy characterizations were performed with a Bruker DSX 500 MHz spectrometer at 14 kHz spinning rate with 1 ms of $\pi/8$ pulse after dehydration for 3 hours at 110 ^{o}C. Framework Si/Al ratios were obtained from ^{29}Si MAS NMR data.

Determination of active Al_2O_3 and SiO_2 contents. By definition, active Al_2O_3 and SiO_2 in calcined aluminosilicate minerals are those formed during the activation, leachable by acid or alkali solution, and can contribute Al and Si species for zeolite synthesis[1]. In the present study, the active Al_2O_3 and SiO_2 contents of the different samples were obtained by leaching 5 g of a sample with 200 mL of a 2 M HCl solution at room temperature for 4 hours, then filtering and washing the leached sample, and finally analyzing the filtrates by inductively coupled plasma - atomic emission spectrometry (ICP-AES).

Chemical composition analyses. Chemical composition analyses of the samples were determined by X-ray fluorescence (XRF) conducted on a Bruker S4 Explorer instrument.

Field-emission environmental scanning electron microscopy (FESEM). The FESEM images of the samples were obtained on a field-emission environmental scanning electron microscope (FEI Quanta 200F).

High resolution transmission electron microscopy (HRTEM). The HRTEM images were taken using a FEI Tecnai F30 (300 kV) high resolution transmission electron microscope with the sample mounted onto a C-flat TEM grid. Digital diffractograms of the BF image and Fourier-filtered image were achieved by using the standard image processing method (Digital Micrograph Program from Gatan Inc.).

Brunauer–Emmett–Teller (BET) characterization. The specific surface areas of the samples were calculated by the BET method, while the external surface areas and microspore volumes (V_{micro}) were estimated using the de Boer t-plot method.

Crystal size. The crystal size was measured by the laser beam scattering technique (Malvern MS2000 Laser particle size analyzer) and FESEM.

Phase structure and relative crystallinity. The X-ray diffraction (XRD) patterns of the samples were obtained on a Bruker AXS D8 Advance X-ray diffractometer with monochromatized Cu Kα radiation (40 kV, 40 mA). The relative crystallinity of the sample was calculated by the ASTM D 3906-03 method.

Structure solution and refinement. XRD data for structure solution and refinement were collected at ambient temperature on a diffractometer (Rigaku D/max-rA12kW). Intensity data were obtained with Cu $K\alpha_{12}$ radiation (λ=1.54056, 1.54033 Å). Tube voltage and current: 40 kV and 100 mA; step scanning size and time: 0.02 (2θ) and 5 s. The 2θ range

goes from 4.00 to 100.00 degrees. The pattern was indexed according to a cubic F unit cell. Then, a Rietveld refinement was performed using the GSAS suite[2], with a visually estimated background and a pseudo-Voigt/FCJ asym profile function. The refined instrument and structure parameters were: cell parameters, scale factor, background, and spherical harmonics of 20th order. The residuals of the refinement were: R_{wp}=0.132, R_p=0.098, R=0.059. The agreement between the observed and calculated patterns is shown in Fig. 3.

Theoretical image. Theoretical image of the Y type zeolite structure was implemented using Accelrys Materials Studio software[3].

Temperature-programmed desorption of ammonia (NH_3-TPD). The strength distributions of the acid sites of the zeolites were studied by NH_3-TPD. First, the zeolite samples, each 200 mg, were heated from room temperature to 600 ^oC at a rate of 10 ^oC/min and then cooled down to 100 ^oC in a pure Ar flow. Then, ammonia was adsorbed at 100 ^oC for 10 min, and subsequently the samples were purged by a flowing Ar stream at 100 ^oC for 1 hour to remove excessive and physically adsorbed NH_3. Finally, the samples were heated from 100 to 600 ^oC at a rate of 10 ^oC/min in a pure Ar flow and the desorption patterns were recorded.

4. Catalytic performance tests

The tests were conducted in a lab scale cracking reactor under the conditions typical for FCC units: cracking temperature 520 ^oC, mass ratio of catalyst to oil 6.5, mass ratio of water to oil 0.29, feed injection time 45 s, and catalyst loading 50 g. Before each test, the system was purged by a N_2 flow (30 mL/min) for 30 min at reaction temperature. After the feed injection, catalyst stripping was performed using a N_2 flow for 15 min. During the reaction and stripping processes, liquid products were collected in a glass receiver kept in an ice-bath, and the gaseous products were collected in a burette by water displacement. Finally, the gaseous products were analyzed on an Agilent 6890 gas chromatograph installed with ChemStation software. The liquid products were analyzed using a simulated distillation gas chromatogram. The coke content was determined by a coke analyzer.

Zeolite activity was determined with cumene as the probe molecule using the pulse cracking method. First, the binder-free HY catalysts were pressed and crushed to particles of the size of 0.2~3 mm. Then, the catalyst (0.1 g) and quartz crumbs (1 g) were placed into the cracking microreactor for dehydration in a nitrogen flow (0.5 mL/h) with the temperature of the reactor being increased up to 400 ℃ at a rate of 20 ℃/min and then being maintained at

400 ℃ for 2 h. Finally, the temperature was decreased to the set value in the range of 240~360 ℃. After the pulses of liquid cumene (3 μL each pulse) were injected into the stream, reaction products were analyzed by an online gas chromatograph installed with a flame ionization detector.

5. Material balance, CO_2 emission, energy consumption analyses and atom economy calculation

The material and energy balance analyses of the traditional synthesis process and the green synthesis process proposed in this study are based on the data of Robson[4] and our results obtained on a 10 L pilot synthesis reactor, respectively. The material consumption was expressed in kilogram. Extraction, processing and transportation of the raw materials are included according to the processes shown in Figs. S10 and S11, all the materials inputs were traced back to the origin. Energy is calculated as the primary energy in calorific values according to Fawer and IPCC[35, 6]. The energy consumption of various transport processes are based on the data of Fawer[5]. The total CO_2 emission (Gg) is expressed by the following equation[6]:

$$\text{Emission} = \sum_{all\ fuels} \left[\begin{array}{l} ((\text{Apparent Consumption}_{fuel} \bullet \text{Conv Factor}_{fuel} \bullet \text{CC}_{fuel}) \bullet 10^{-3} \\ -\text{Excluded Carbon}_{fuel}) \bullet \text{COF}_{fuel} \bullet \dfrac{44}{12} \end{array} \right]$$

where, Apparent Consumption is equal to (production + imports – exports – international bunkers - stock change); Conv Factor (conversion factor) refers to conversion factors for the fuel to energy units (TJ) on a net calorific value basis; CC refers to carbon content (tonne C/TJ, C/TJ is identical to kg C/GJ); Excluded Carbon refers to carbon in feedstocks and for non-energy use which do not directly released into the atmosphere as greenhouse gases (Gg C, $\text{Excluded Carbon}_{fuel} = \text{Activity Data}_{fuel} \bullet \text{Carbon Content}_{fuel} \bullet 10^{-3}$); COF (carbon oxidation factor) refers to the fraction of carbon oxidized. Usually, COF value equals 1, reflecting complete oxidation.

When considering a waste water emission, only the inorganic salts and organic compounds contained are counted, with water excluded.

Atom economy was calculated by dividing the molecular weight of the desired product by the sum of the molecular weights of all substances produced in the stoichiometric equation[7].

Supplementary Tables

Table S1. The production processes of sodium silicate solution and aluminum hydroxide: mass and energy balance analyses.

Item	Soluble sodium silicate (37% solid), /kg product	Aluminum hydroxide, /kg product
Raw materials		
Quartz, kg	0.287	-
Bauxite, kg	-	1.257
Limestone, kg	0.190	0.059
Rock salt, kg	0.237	0.040
Water consumption, kg	115.00	
Wastes		0.048
Solids emission, kg	0.236	0.011
Water emission, kg	0.425	0.676
CO_2 emission, kg	4.623	11.633
Total energy consumption, MJ	4.623	0.287

Note: Data were adapted from Fawer, M. *et al*[5, 8]. The SiO_2 and Na_2O contents in the soluble sodium silicate are 28.4 wt% and 8.6 wt%, respectively.

Table S2. Chemical compositions of the kaolinite and diatomite minerals, the as-synthesized zeolite Y and commercial zeolite Y.

Component, wt%	Na_2O	Al_2O_3	SiO_2	P_2O_5	SO_3	MgO	K_2O	CaO	TiO_2	Fe_2O_3
Kaolinite	2.8	44.6	50.5	0.2	0.3	0.1	0.4	0.1	0.3	0.5
Diatomite	0.7	3.2	93.6	0.1	0.3	0.1	0.7	0.2	0.2	1.1
As-synthesized zeolite Y	11.2	20.1	67.2	0	0.1	0.1	0.5	0.2	0.1	0.3
commercial zeolite Y	9.6	22.3	67.8	0	0.1	0.1	0.1	0.1	0	0.1

Table S3. Physicochemical properties of the as-synthesized zeolite Y and the commercial zeolite Y.

Sample	As-synthesized zeolite Y	Commercial zeolite Y
BET area , m^2/g	703	728
Micropore area, m^2/g	627	663
External surface area, m^2/g	76	65
Crystal size, μm	0.6 ~ 0.7	1.5 ~ 1.8
Relative crystallinity, %	92	100
Framework SiO_2/Al_2O_3 molar ratio	5.0	5.0
Bulk density, g/mL	0.42	0.37

Table S4. Properties of the Xinjiang vacuum gasoil.

Item	Xingjiang vacuum gasoil
Density (293 K), kg/m^3	898.40
Kinematic viscosity at 373 K, mm^2/s	12.05
Average molecular weight, g/mol	449
Conradson carbon residue, wt%	0.39
Lumped composition, wt%	
Saturated alkanes	76.59
Aromatics	21.01
Resins	4.08
Asphaltenes	0.17
Element composition, wt%	
C	86.02
H	13.13
N	0.12
S	0.64

Table S5. Product yield and atom economy for zeolite Y synthesis.

Item	Green process proposed in this investigation /kg zeolite Y	Traditional process, /kg zeolite Y
Raw materials		
Quartz, kg	0	1.291
Bauxite, kg	0	0.489
Diatomite, kg	1.066	0
Kaolinite, kg	0.327	0
Rock salt, kg	0.370	1.212
Limestone, kg	0	0.878
Intermediates		
Sodium silicate solution (28.7 wt% SiO_2) , kg	0	4.498
Aluminum hydroxide, kg	0	0.389
Activated diatomite, kg	1.014	0
Activated kaolinite, kg	0.667	0
NaOH, kg	0.189	0.220
Soda, kg		0.670
Zeolite yield*, %	69.46	63.58
Energy consumption†, MJ	35.688	46.259
Solid waste emission, kg	0.048	0.386
Waste water emission, kg	0.053	1.104
CO_2 emission, kg	1.860	3.236
Atom economy‡, %	50.91	32.79

Notes:

*Yield (g/g) is defined as the ratio of the weight of calcined zeolite to the dry weight of Al_2O_3 and SO_2 in the synthesis system[9].

Supplementary Figures

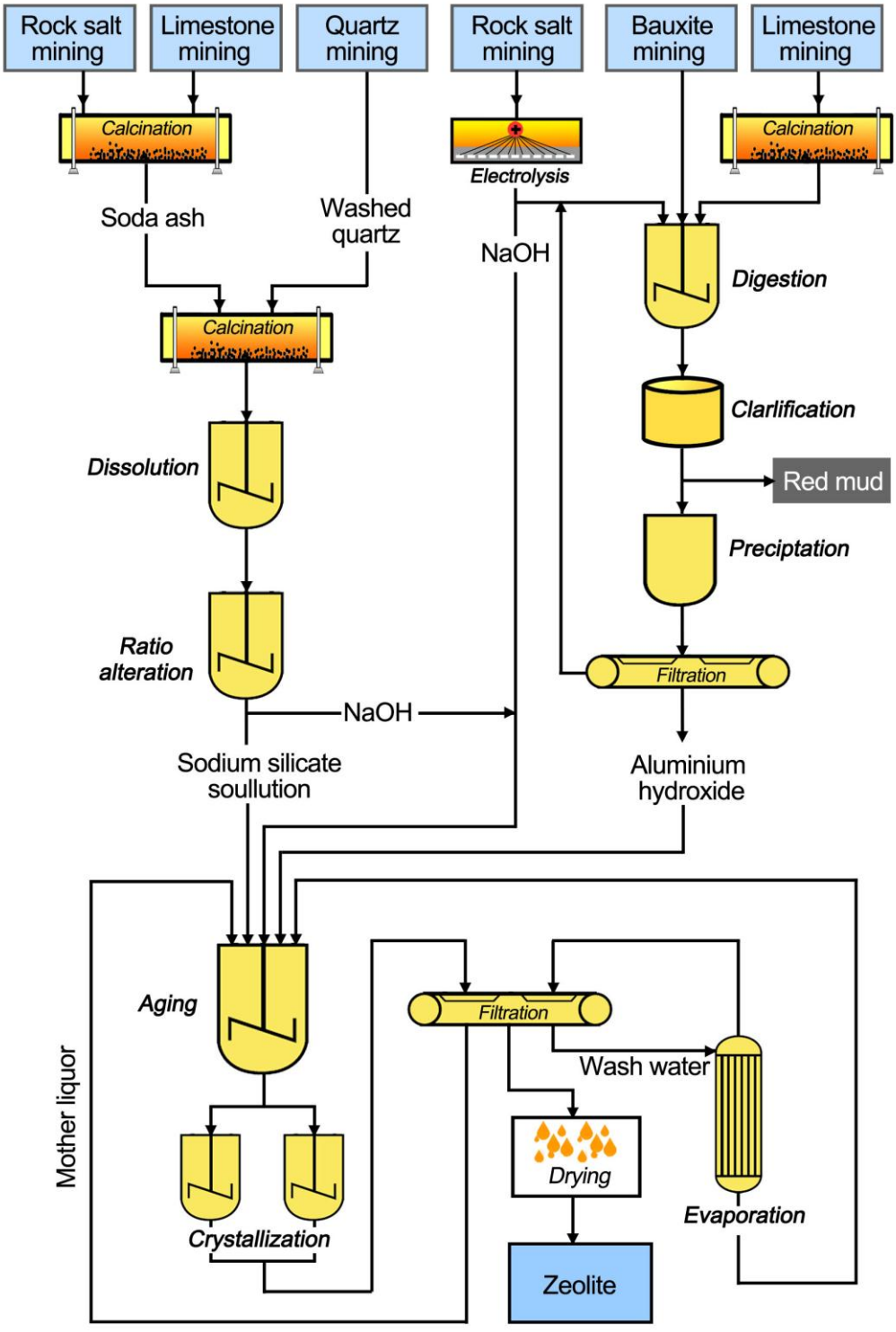

Figure S1. Manufacturing process of aluminosilicate zeolites by the conventional method.

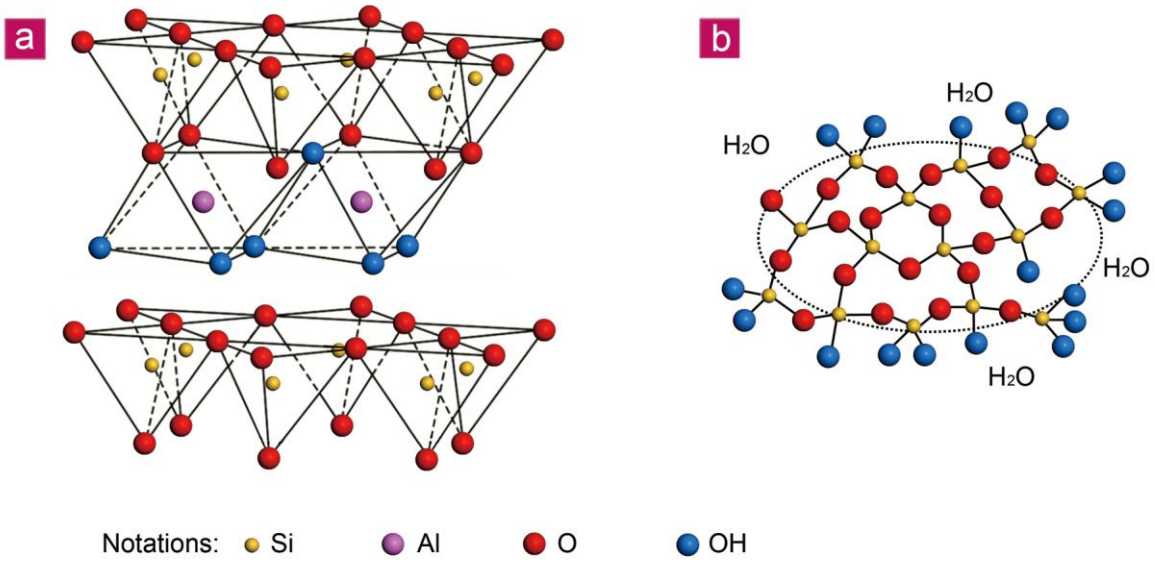

Figure S2. Schematic illustration of the framework structures. a, kaolinlite. **b,** diatomite.

Figure S3. Active Al_2O_3 and SiO_2 contents in the samples. a, the HCAS activated kaolinite. **b,** the thermally activated kaolinite. The digital camera images of the samples show that the whole HCAS activated kaolinite sample was nearly dissolved in the HCl solution, but only a small part of the thermally activated kaolinite sample was dissolved in the same HCl solution. The further analysis of the filtrates by the ICP-AES method demonstrates that the HCAS activated kaolinite has higher active Al_2O_3 and SiO_2 contents than the thermally activated kaolinite sample, 99.3 wt% and 98.9 wt% *vs*. 7.5 wt% and 2.1 wt%.

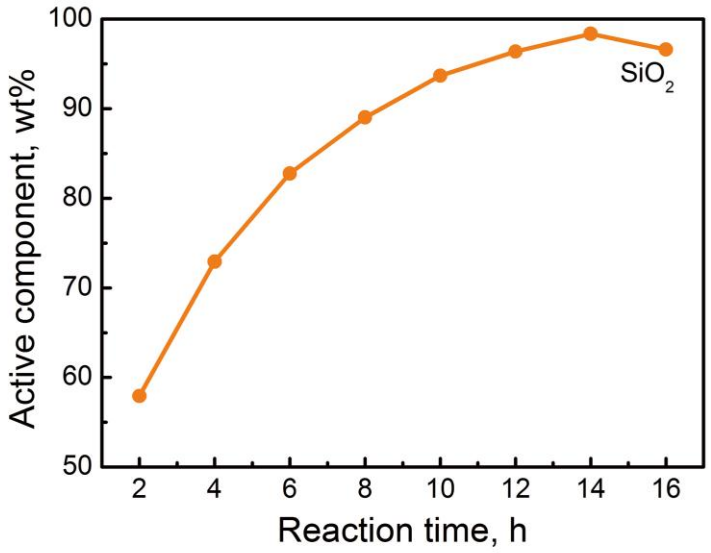

Figure S4. The content of the dissolvable silica in the thermally activated diatomite as a function of time in 1.3 M NaOH at 60 ^{o}C.

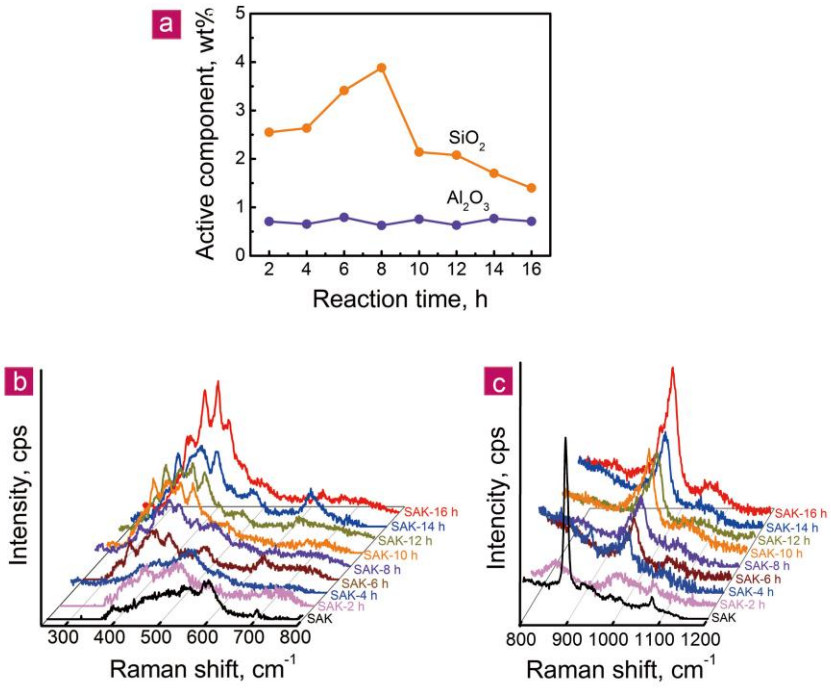

Figure S5. The reaction between the HCAS activated kaolinite and water. a, the contents of the dissolvable silica and alumina in the HCAS activated kaolinite as a function of time in water at 60 ^{o}C. **b,** Raman spectra (the low-frequency region) of the HCAS activated kaolinite and its solid products formed after 2 to 16 hours of reaction in (a). **c,** Raman spectra (the high-frequency region) of the HCAS activated kaolinite and its solid products formed after 2 to 16 hours of reaction in (a). SAK-*m*h denotes the solid product of the HCAS activated kaolinite dissolved in water after reaction for *m* hours at 60 ^{o}C. It should be noted that after the HCAS activated kaolinite reacted with water, there are four peaks in the wavenumber range of 350~500 cm^{-1}, and the intensity of peaks increases with the increasing reaction time, resulting from the transformation of the initial solids into tectosilicates fabrics that contain five- and six-membered aluminosilicate rings[10, 11] and act as the precursors for nucleation[12]. As the reaction proceeds, we can also observe an increase in the peak intensity at 980 cm^{-1} which is assigned to the vibration of Si-OH along with the disappearance of the peak at 890 cm^{-1} that is characteristic of the vibration of Si-O^{-}····Na^{+}, indicating that the hydration of Na^{+} in the HCAS activated kaolinite followed by hydrolysis of Si-O^{-}····Na^{+} linkages and formation of Si-OH. The Raman spectra of the samples further highlight that the HCAS activated kaolinite has high reactivity and can spontaneously transform into polymerized aluminosilicates with tectosilicates fabrics, while the silica and alumina species do not have to be present in solution before being incorporated into a growing secondary phase.

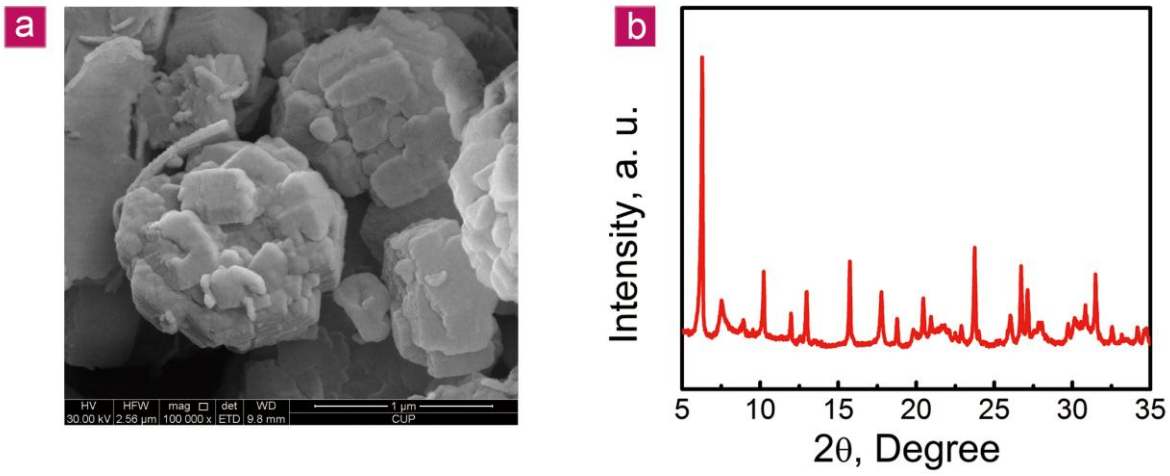

Figure S6. Characterization of the product synthesized from the thermally activated kaolinite and thermally activated diatomite. a, FESEM images. **b,** XRD pattern. As shown in figure S6, the product obtained from the thermally activated kaolinite and thermally activated diatomite has irregular morphology and contains a significant amount of phase impurities, typically some unreacted mineral flakes.

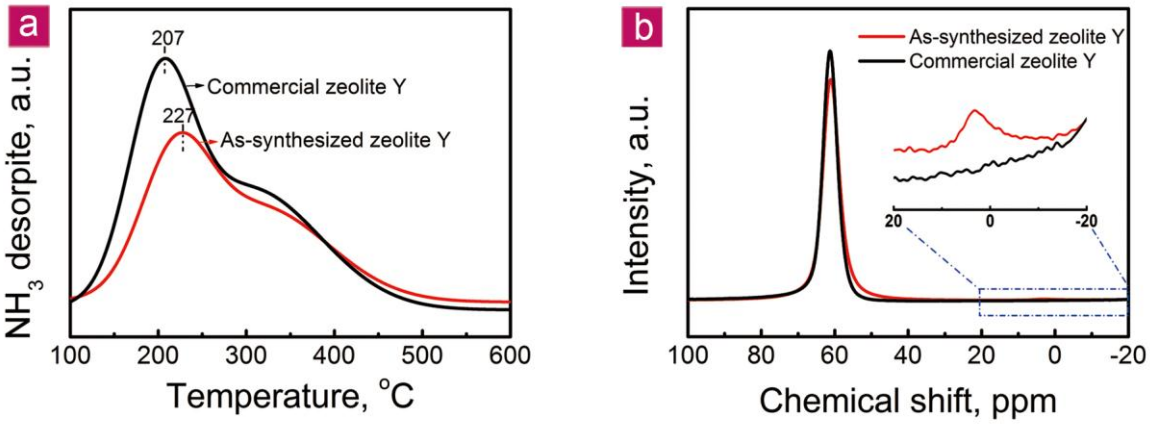

Figure S7. Acidity characterization results. a, the NH_3-TPD curves of the as-synthesized zeolite and the commercial zeolite Y. The results show that compared with that of the commercial zeolite Y, the as-synthesized zeolite Y has stronger acid strength which gave the higher cracking activity despite of its relatively less amount of acid sites. **b,** ^{27}Al MAS NMR spectra of the as-synthesized zeolite and the commercial zeolite Y. The stronger acid strength of the as-synthesized zeolite Y is probably induced from extra-framework Al species associated with Si-OH-Al groups**.**

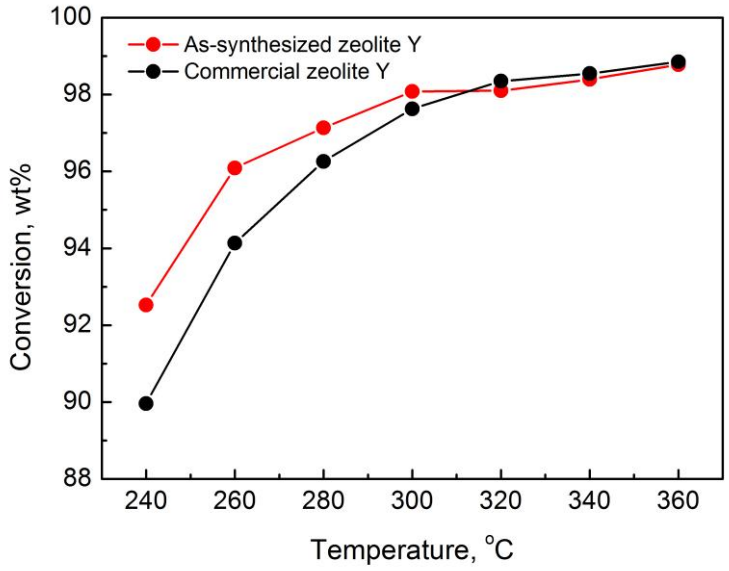

Figure S8. Activity of the as-synthesized zeolite Y and commercial zeolite Y for the catalytic conversion of cumene. The catalytic results show that the as-synthesized zeolite gave higher cumene conversion than the commercial zeolite Y, demonstrating again the superior catalytic performance of that the as-synthesized zeolite.

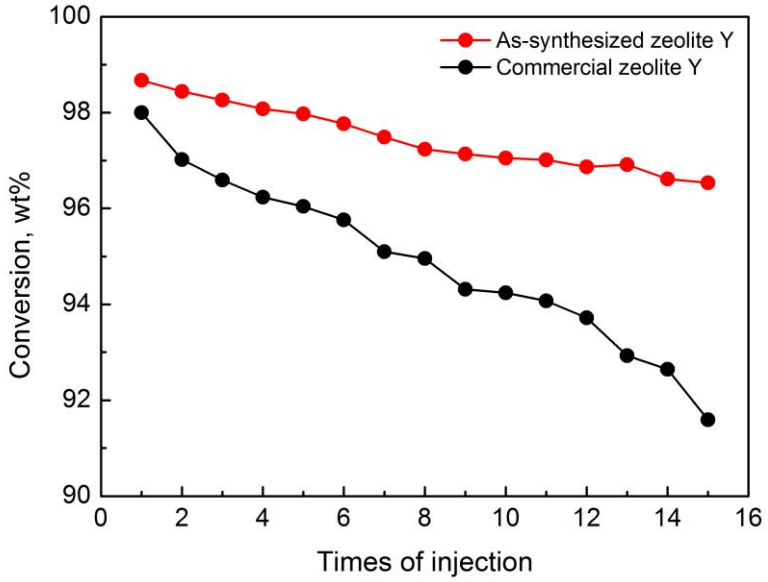

Figure S9. Deactivation behavior of the as-synthesized zeolite Y and commercial zeolite Y for the catalytic conversion of cumene at 340 ^{o}C (0.5 μL of cumene was injected for each test). The deactivation characteristic results show that the as-synthesized zeolite exhibited slower deactivation ratio than the commercial zeolite Y.

Supplementary References

1. B. Wei, H. Liu, T. Li, L. Cao, Y. Fan and X. Bao, *AIChE J.*, 2010, **56**, 2913-2922.
2. A. C. Larson and R. B. V. Dreele, *General structure analysis system (GSAS)*, Los Alamos National Laboratory Report LAUR, 2004.
3. *ACCELRYS Corp.: San Diego, CA.*, 2002.
4. H. Robson, *Verified syntheses of zeolitic materials*, Elsevier Science B.V., Amsterdam, 2001.
5. M. Fawer, *Life cycle inventory for the production of zeolite A for detergents*, Report EPMA 234, St. Gallen, 1996.
6. *2006 IPCC guidelines for national greenhouse gas inventories*, Institute for Global Environmental Strategies, Hayama, Japan, 2006.
7. R. A. Sheldon, S. Arends and U. Hanefeld, *Green chemistry and catalysis*, WILEY-VCH, Weinheim, 2007.
8. M. Fawer, M. Concannon and W. Rieber, *Int. J. LCA*, 1999, **4**, 207-212.
9. B. A. Holmberg, H. Wang, J. M. Norbeck and Y. Yan, *Microporous Mesoporous Mater.*, 2003, **59**, 13-28.
10. W. H. Casey, H. R. Westrich, J. F. Banfield, G. Ferruzzi and G. W. Arnold, *Nature*, 1993, **366**, 253-256.
11. Y. Kamimura, S. Tanahashi, K. Itabashi, A. Sugawara, T. Wakihara, A. Shimojima and T. Okubo, *J. Phys. Chem. C*, 2011, **115**, 744-750.
12. S. Mintova, N. H. Olson and T. Bein, *Angew. Chem., Int. Ed.*, 1999, **38**, 3201-3204.